Journal of Environmental Sciences Studies

Journal home page: www.jess.ir

Catalytic degradation of organic dyes using eggshell-derived hydroxyapatite coated by silver nanoparticles

Hossein Yarahmadi[1*]

[*]1- Department of Chemical Engineering, Sirjan University of Technology, Sirjan, 7813733385, Iran
Email Address: hyarahmadi61@gmail.com

Received: (2022-12-01)
Accepted: (2023-01-14)

Abstract

Developing chemical remediation techniques has become an increasingly important research topic due to the growth in the use of organic dyes which can be harmful to nature and human health. Catalytic reduction reaction of organic pollutant dyes (OPDs) in the presence of metal nanoparticles (MNPs) such as copper, silver and palladium is an efficient and simple method to treat polluted industrial waters. However, easily agglomeration of the MNPs impacts their efficiency and re-usability. Therefore, we used chicken eggshells as a natural resource to make hydroxyapatite (HAP) as a heterogeneous bed with high contact surface by friendly hydrothermal and environmentally method. The HAP was coated with silver nanoparticles (AgNPs@HAP) and was used as an efficient and recyclable catalyst for the reduction of OPDs (Methylene blue (MB), 4-Nitrophenol (4-NP) and 4-Nitroaniline (4-NA)) in the presence of sodium borohydride. The reduction reaction was performed in less than 10 minutes with excellent efficiency (approximately 100%) and the reaction kinetics were investigated by change of the absorption intensity using a two-beam UV-Vis spectrophotometer. The physical and chemical properties of AgNPs@HAP were evaluated and the prepared solid heterogeneous catalyst was characterized via FTIR, XRD, BET, TEM, FE-SEM/EDS and elemental mapping analysis. This study demonstrates the potential use of HAP derived from biowaste eggshell with high efficiency for the degradation of OPDs under mild reaction conditions at room temperature. In addition, AgNPs@HAP showed high stability and reusability for four cycles with almost constant catalytic performance.

Keywords: Pollutants, degradation, organic pollutant dyes (OPDs), silver nanoparticles, hydroxyapatite

1. Introduction

Large volumes of effluent are produced daily by industries such as textiles, cosmetics, printing and dye production. If these polluted effluents are not treated, they can enter surface and groundwater resources that in turn can have devastating and irreversible effects on human health and the ecosystem [1]. Therefore, water and wastewater treatment has become one of the major global concerns.

Aromatic organic dyes and pigments are the most common toxic pollutants among industrial effluents, which are often not biodegradable [2]. For example, 4-NP is a hazardous and carcinogenic organic dye that is very stable in water and difficult to decompose environmentally [3]. In addition to irritating the eye, this aromatic colour pollutant can cause severe kidney and liver dysfunction, which has led the US Environmental Protection Agency to blacklist it [3, 4].

Today, various methods such as physical, chemical and biological treatment are used to remove hazardous and toxic pollutants from polluted effluents and waters [5, 6]. Examples include membrane filtration, oxidation, light or chemical degradation, coagulation, flocculation, biodegradation, and catalytic reduction [5-7]. The catalytic reduction method is an alternative method that has been reported to be a cheap, fast and more efficient method for the treating of water containing OPDs.

However chemical compounds such as hydrazine and are among the catalysts that can reduce OPDs such as 4-NP, 4-NA and MB [8-10], but these substances are hazardous and produce secondary pollutants that can be harmful to the environment. On the other hand, although reduce agents such as sodium borohydride ($NaBH_4$) alone is unable to reduce the mentioned pollutant compounds, but it can perform the reduction process in the presence of metal catalysts completely. Up to now, some of the metal catalysts such as silver, copper and palladium nanoparticles were applied to reduce OPDs with acceptable efficiency and kinetics [11-14].

However MNPs can be used for the preparation of catalysts to increase significantly their catalytic activity but these particles have high tendency to accumulate and aggregate [15, 16]. Therefore, they are often dispersed and stabilized on heterogeneous

substrates to prevent agglomeration [15-18]. Today, the development of solid substrates has been considered especially by researchers, industrial chemical production and environmentalists. Solid substrates should have characteristics such as high thermal stability and good access to active sites. Numerous heterogeneous substrates, especially environmentally friendly substrates, have been proposed and used by researchers to stabilize MNPs[17].

In recent years, to prevent the production of secondary pollutants, researchers have especially used biowastes such as lignin [19-22], animal bones [23, 24] and eggshells [25-27] to the preparation of solid substrates such as hydroxyapatite (HAP) in the catalytic reactions. HAP is a bioceramic material with the molecular formula of $Ca_{10}(PO_4)_6(OH)_2$. In addition to being biocompatible, HAP has a high porosity, surface contact, mechanical, chemical and thermal stability [28]. So far, it has been widely used in various medical and chemical fields such as bone reconstruction, tooth restoration and suitable and recyclable substrate for the preparation of heterogeneous adsorbents and catalysts [25-30]. Up to now, various methods such as hydrothermal method, sol-gel process, mechanical method, microwave synthesis and wet chemical deposition method have been proposed to produce HAP [30]. Annually millions of eggshells are dumped or buried as waste in the environment that can be used as a cheap and available precursor to the preparation of hydroxyapatite, which can be a "trash to treasure" process. Therefore, using eggshell as a raw material is one of the most common methods for the preparation of HAP.

In this study, eggshell derived HAP was prepared via a simple and green process and used as a solid substrate for the stabilization of silver nanoparticles. Finally, eggshell derived hydroxyapatite coated by silver nanoparticles (AgNPs@HAP) was applied as a catalyst in reduction reaction of some OPDs (4-NP, 4-NA and MB) in the presence of NaBH4 at room temperature. The obtained results show that OPDs can be reduced in the presence of AgNPs@HAP in high yield along a short time.

2. Experimental procedure

2.1. Materials

The used eggshells were collected from locally restaurants and confectioneries. Phosphoric acid, Sodium hydroxide, n-Hexane, Ammonium chloride, 4-NP, 4-NA and MO were prepared by Merck and Aldrich Chemical and used without further refining.

2.2. The preparation of HAP

HAP was prepared from biowaste eggshells based on the reported method by Shi et al. [31] with minor modifications (Scheme 1). At first, eggshells were collected from locally restaurants and confectioneries in Sirjan City which produce daily a large number of eggs to make omelets and sweets. To remove organic matter, membranes and excess particles, the collected eggshells are boiled and washed for 2 hours in water and hexane solvents under reflux conditions and dried for 5 hours at 90 ° C. Dried eggshells were then grounded in a mortar and a white powder of eggshells was obtained (ES1). To obtain an equal molar ratio of calcium and phosphorus, 5 g white powder ES1 and 6 mL phosphoric acid (85 %) were added to 50 mL deionized water and was exposed to ultrasonic for 30 minutes at 50 °C. By performing the reaction, the releasing of carbon dioxide gas from the reaction medium is easily visible in this step of the procedure. Finally, the obtained suspension of calcium phosphate ($CaHPO_4$) was centrifuged (4000 rpm). Obtained calcium phosphate was added to 50 mL deionized water, then was stirred 30 min (500 rpm) to prepare a white suspension (ES2).

Please insert Scheme 1.

Elsewhere, 5 g of ES1 was calcined for 4 hours at 900 °C in an electric furnace to form calcium oxide (CaO). By addition of 50 mL deionized water to the CaO, calcium hydroxide suspension was formed during an exothermic reaction (ES3). The suspension (ES3) was added dropwise to ES2 (suspension of of calcium phosphate ($CaHPO_4$)) and stirred at ambient temperature for 1 hour using a magnetic stirrer (750 rpm). At this step of the total procedure, sodium hydroxide solution (10% w/w) was used to stabilize the alkaline suspension's pH in the range of 12-13. The suspension was transferred into an autoclave with a Teflon coating and heated at 180 °C for 3 hours. The resulting hydroxyapatite was centrifuged (4000 rpm), washed with 1% ammonium chloride solution and dried overnight at 95 °C (bulk-HAP).

2.3. The preparation of HAP coated by silver nanoparticles (AgNPs@HAP)

AgNPs@HAP was prepared via the ball milling of precursors (bulk-HAP and AgNO3). At first, 2 g bulk-HAP was mixed with 2 mg $AgNO_3$ and introduced into a hardened steel vial (vol. 50 mL). The resulted powder was ball-milled for 2 h by hardened chromium balls (2×15 mm and 2×10 mm, the total mass of 2.5 g) under air atmosphere using a high-energy planetary ball mill running at 500 rpm with the absence of process control agents. The ball-to-powder mass ratio was consistently kept at about 5:1 for all experiments. The milled white powder was poured into 100 mL of deionized water and vigorously stirred at 1000 rpm for 15 minutes at room temperature. Then, 25 mL of sodium borohydride solution (0.1 M) was added and stirred for 1 hour to reduction of silver ions. The Prepared AgNPs@HAP was centrifuged (4000 rpm) and washed several times with deionized water to remove unreacted materials. Obtained AgNPs@HAP

was dried in an electric oven at 90 °C for 24 h and was applied as a catalyst for the reduction of OPDs at room temperature in aqueous medium.

Please insert Scheme 2.

2.4. Devices and Characterization

A high-energy ball mill model 2021 produced by Isfahan San'at Company was used to grind and UV-Vis absorption spectra were obtained using a UV-4802 Unico instrument. Characterization of the catalytic composite was subjected by using Fourier Transform Infrared Spectroscopy (FTIR) (KBr), Field Emission Scanning Electron Microscope (FESEM), X-ray diffraction (XRD), Brunauer-Emmett-Teller (BET) and Brunauer-Joyner-Hallenda (BJH), Transmission Electron Microscopy (TEM), Energy Dispersive Spectroscopy (EDS) and elemental mapping analysis. A JASCO 6300 spectrophotometer was employed for the recording of FT-IR spectra in the range of 400-4000 cm^{-1}. FESEM images and EDS analysis were recorded via TESCAN BRNO-Mira3LMU with a voltage of 15.0 kV and TEM images were obtained using Philips EM 208S. For XRD analysis, D8-ADVANCE Bruker apparatus with graphite monochromatic Cu-Kα was applied to determine the structure of the synthesized AgNPs@HAP in the range of 10-90° with a scanning speed of 2° per minute. The specific surface area (SSA) and pore size distribution of AgNPs@HAP were determined on a BEL-SORP-mini2 analyzer based on the data of N_2 adsorption-desorption isotherms in BET analysis.

2.5. General procedure and catalytic efficiency of $AgNPs@NO_3$ in reduction reaction of OPDs

In a general experiment, 20 mL of aqueous dye solution (20 ppm) was mixed with a required volume of freshly prepared aqueous NaBH4 (0.1 M) (20-40 mL). Because of auxochromic nature of 4-NP, bright yellow solution would be changed to deep yellow in this step. Then, 20 mL of aqueous solution of AgNPs@HAP (10-40 ppm) was added rapidly to the obtained solution. The color intensity of the solution would be decreased and finally a colorless solution is obtained. During the reaction time, at constant intervals, 5 mL volumetric samples were taken from the reaction mixture and after catalyst separation, catalytic reduction of OPDs was detected by measuring the absorption changes at the corresponded λ_{max} by a dual-beam Uv-Vis spectrophotometer (Figure 1).

Please insert Figure 1.

Because of exochromic properties of 4-NP, its adsorption peak changes from 320 nm (4-NP (a)) to 400 nm after addition of sodium borohydride (4-NP (b), Fig. 1).

3. Results and discussion

3.1. Characterization of AgNPs@HAP

The FT-IR spectrum of AgNPs@HAP was obtained to confirm the functional groups and chemical structures of AgNPs@HAP. The results are in agreement with the literature [32-34]. As shown in Figure 1, spectrum of AgNPs@HAP show the characteristic FT-IR absorption peaks related to the functional groups and bands positions at 3430, 1630, 1420, 1040, 956, 873, 603 and 571 cm^{-1}.

Please insert Figure 2.

FT-IR spectra of the AgNPs@HAP show peaks at 500 to 600 cm^{-1} which is attributed to the presence of metal in the nanoparticle. Three modes of absorption related to PO_4^{-3} functional group can be seen in the FT-IR spectrum: degenerated asymmetric mode at 1040 cm^{-1}, the non-degenerated symmetric mode at 956 cm^{-1}, and the bending mode at 603 and 571 cm^{-1}. The peak observed around 3430 cm^{-1} corresponded to the characteristic OH stretching vibration of HAP. In addition, a band at approximately 1630 cm^{-1}, as well as a broad band from 2500-3500 cm^{-1}, could be ascribed to the bending and symmetric stretching vibration of absorbed H_2O. These peaks might be related to $CaHPO_4{\cdot}2H_2O$ in produced HAP. Two peaks approximately at 1420 cm^{-1} and 873 cm^{-1} were significantly assigned to the stretching vibration and bending absorption of carbonate ions, respectively.

In addition, Figure 2 shows the XRD pattern of the AgNPs@HAP composite. The XRD pattern shows that it contains major peaks at 2θ = 25.7°, 29.5º, 31.6°, 32.1°, 33.9°, 39.9°, 49.4°, 53.0°, 64.0°, 76.9° and 83.5°. As was shown in Figure 3, according to the standard JCPDS card No. 96-901-3628, the obtained XRD pattern for the prepared composite matched well with that for pure crystal hydroxyapatite. The XRD image of AgNPs@HAP represents peaks with different intensities, which confirms the modifications of HAP. Also, new peaks including a peak attributed to the Ag solid phase were found in this XRD diffractogram.

Please insert Figure 3.

The presence of Ag in EDS and elemental mapping analysis confirm the presence of Ca, O, P, and Ag elements as shown in Figure 4 in the composition of AgNPs@HAP. FESEM analysis was performed to determine the morphology of AgNPs@HAP (Figure 5). According to this analysis, the surface of the sample is relatively homogeneous with fine particles and the catalyst particle size is in the nanometer range with irregular morphology.

Please insert Figure 4.
Please insert Figure 5.

The BET-SSA is an important item because it is related to the active site of the catalysts. Using ultra-

high purity grade (99.999%) gases, the BET analysis was applied (P/P_o = 0.005-1.00) and all gas sorption isotherms were obtained consistent with the consistency criteria for microporous materials (Figure 6).

Please insert Figure 6.

Before analysis, the as-prepared solid sample (HAP or AgNPs@HAP) (0.2-0.5 g) was first solvent-exchanged using EtOH, then pre-treated in the analysis tube in an oven and outgassed under vacuum (down to 5-8 bar) with heating up to 200 ºC. The BET-SSA and the pore diameter of HAP and AgNPs@HAP derived from ES are listed in Table 2. Compared with BET-SSA of eggshell (1.91 m^2g^{-1}) [35], the BET-SSA of the eggshell-derived HAP increased significantly to 64.03 m^2g^{-1} which these values are far greater than the values of two commercialized HAPs including technical grade HAP (51.39 m^2g^{-1}) and biological reagent HAP (35.09 m^2g^{-1}) [36]. The ranking of pore volume also existed in the same phenomenon. Moreover, synthesized HAP samples at high temperatures (ball-milled HAP) had larger SSA and higher pore volume than the coated HAP (AgNPs@HAP). It seems that the Ag coating of HAP samples effects radically on their surface areas. After the coating of HAP by AgNO3, the mean pore diameter of particles increased from 28.41 to 31.08 nm and SSA decreased from 62.15 to 56.03 m^2g^{-1} (Table 1). Therefore, eggshell-derived HAP presented a great SSA and pore volume that has good pore characteristics of porous structure and it is an ideal candidate for various applications such as adsorbents or solid substrates for the preparation of heterogeneous catalysts [37-42].

Please insert Table 1.

From the TEM observations, they were clear that the mesoporous structure of AgNPs@HAP was well sustained (Figure 7). Based on TEM analysis, it can result that no obvious extra phases of HAP species were present outside the mesoporous AgNPs@HAP. It confirms that Ag is well supported on mesoporous carrier HAP.

Please insert figure 7.

3.2. Catalytic degradation of OPDs in the presence of AgNPs@HAP

In the contaminant organic dye reduction reactions, as the reaction time progressed, with the decrease of the contaminant organic dye concentration, the soluble dye disappeared in a short time (6-12 min) under experimental conditions. The adsorption intensity decreased at the maximum wavelength of the dye composition. Moreover, the reaction kinetics of reduction and degradation of the applied dyes were monitored and analyzed by plotting the concentration of the contaminant organic dye against the reaction time. Since the concentration of sodium borohydride is much higher than the concentration of the dye used, the reduction process was considered a quasi-first-order reaction. According to Equation 1 and the relationship between adsorption intensity and reactant concentration in a quasi-first-order reaction, the Ln ($[C_t]/[C_o]$) graph was plotted as a function of reaction time. As shown in Figure 8, the measured data are fitted to a linear trend line and the reaction rate constant (k, min^{-1}) was obtained by calculating the slope of the line. $[C_o]$ and A_o represent the concentration and intensity of adsorption at the initial moment of the reaction, and $[C_t]$ and A_t represent the same values during the reaction. k is also a constant display of reaction speed.

$$\text{Ln}((A_t)/(A_o)) = \text{Ln}([C_t]/[C_o]) = -kt \qquad (1)$$

Because of the large difference between the donor (sodium borohydride) and receptor (dye composition) levels, the reduction reaction in the absence of the catalyst takes place by a very small percentage after 4 h, and the adsorption intensity at λ_{max} remains almost constant. This suggests that the reduction reaction is limited in the catalyst absence. When AgNPs@HAP was added to the mixture of applied dyes and sodium borohydride, the adsorption peak almost disappeared completely, indicating that the dye reduction reaction in the presence of sodium borohydride and catalyst coexistence was successful. This indicates that AgNPs@HAP particles were able to transfer electrons from donor to receiver.

The reduction results of methylene blue and 4-NP in the presence of AgNPs@HAP are compared with other catalysts reported in the literature in Table 2. The results in Table 2 show the high performance of AgNPs@HAP without the use of expensive reagents to reduce MB and 4-NP. It should be noted that the specific surface area and high contact of AgNPs@HAP increase dye adsorption and increase the rate of degradation reaction.

Please insert Table 1.

3.3. Recovery and reusability of the catalyst

The stability and reusability of catalysts are great importance for their long-term and multiple applications. Therefore, to investigate the recyclability of the AgNPs@HAP catalyst after its degradation with $NaBH_4$, it was centrifuged and recovered from the reaction mixture after washing it with ethanol. The results are presented in Figure 9.

Please insert figure 9.

The results in Figure 9 showed that the recycled catalyst retains a significant amount of catalytic activity even after five consecutive cycles. The slight decrease in efficiency can be attributed to the loss of

the catalyst during the catalyst recovery process from the reaction mixture. This work offers new insights into the construction of stable HAP-based catalysts with biomass-derived components for the effective degradation of organic contaminants in aqueous solutions.

4. Conclusion

In summary, a simple and environmentally friendly strategy for the preparation of a combination of AgNPs@HAP from eggshell biomass with $AgNO_3$ is presented. AgNPs@HAP was used to degrade contaminants in aqueous media at room temperature. The results show high catalytic activity of AgNPs@HAP in reducing of contaminant dye compositions. The proposed catalyst can degrade the organic dyes such as MB, 4-NP and 4-NA in the presence of sodium borohydride in a short time (less than 12 minutes). In addition, after five consecutive cycles, the catalytic activity of the recycled catalyst was more than 96%, indicating the excellent stability and recyclability of AgNPs@HAP. These results showed that AgNPs@HAP can act as a high-performance heterogeneous catalyst to reduce organic dyes.

Acknowledgements

We thank the Sirjan University of Technology for supporting this research

Nomenclature

4-NA	4-Nitroaniline
4-NP	4-Nitrophenol
MB	Methylene blue
HAP	Hydroxyapatite
XRD	X-ray Diffraction
MNPs	Metal Nanoparticles
SSA	Specific Surface Area
OPDs	Organic Pollutant Dyes
BET	Brunauer-Emmett-Teller
BJH	Brunauer-Joyner-Hallenda
EDS	Energy Dispersive Spectroscopy
TEM	Transmission Electron Microscopy
FTIR	Fourier Transform Infrared Spectroscopy
FESEM	Field Emission Scanning Electron Microscopy

5. References

1. Ismail, G.A. and H. Sakai, Review on effect of different type of dyes on advanced oxidation processes (AOPs) for textile color removal. Chemosphere, 2022. **291**: p. 132906.
2. Schwitzguébel, J.P., et al., Sulphonated aromatic pollutants. Limits of microbial degradability and potential of phytoremediation. Environ Sci Pollut Res Int, 2002. **9**(1): p. 62-72.
3. Guo, Y., et al., Polyvinylpyrrolidone and graphene-modified hematite nanoparticles for efficient electrocatalytic oxidation of p-nitrophenol. Journal of Solid State Electrochemistry, 2022. **26**(4): p. 1051-1065.
4. Lin, C., et al., Ni nanoparticles-loaded ZnO nanowire as an efficient and stable catalyst for reduction of 4-nitrophenol. EcoMat, 2022. **4**(2): p. e12164.
5. Bognár, S., P. Putnik, and D. Šojić Merkulov, Sustainable Green Nanotechnologies for Innovative Purifications of Water: Synthesis of the Nanoparticles from Renewable Sources. Nanomaterials, 2022. **12**(2).
6. Baig, U., M. Faizan, and M. Sajid, Effective removal of hazardous pollutants from water and deactivation of water-borne pathogens using multifunctional synthetic adsorbent materials: A review. Journal of Cleaner Production, 2021. **302**: p. 126735.
7. Kumar, R., et al., A review on emerging water contaminants and the application of sustainable removal technologies. Case Studies in Chemical and Environmental Engineering, 2022. **6**: p. 100219.
8. Abd El Maksod, I.H. and T.S. Saleh, The use of nano supported nickel catalyst in reduction of p-nitrophenol using hydrazine as hydrogen donor. Green Chemistry Letters and Reviews, 2010. **3**(2): p. 127-134.
9. Goswami, N., et al., Kinetic studies on the catalytic reduction of o-, m-, and p-nitrophenols by hydrazine. Journal of Chemical Technology and Biotechnology. Chemical Technology, 1984. **34**(5): p. 195-202.
10. Fan, M., et al., Mn3O4/N-Doped Graphite Catalysts from Wastewater for the Degradation of Methylene Blue. Chemistry – A European Journal, 2018. **24**(54): p. 14554-14559.
11. Ningsih, L.A., et al., Ag-modified TiO2/SiO2/Fe3O4 sphere with core-shell structure for photo-assisted reduction of 4-nitrophenol. Environmental Research, 2022. **214**: p. 113690.
12. Wu, Z., et al., Spherical covalent organic framework supported Cu/Ag bimetallic nanoparticles with highly catalytic activity for reduction of 4-nitrophenol. Journal of Solid State Chemistry, 2022. **311**: p. 123116.
13. Durán, B., et al., Novel 3D copper nanoparticles/chitosan/nanoporous alumina (CCSA) membranes with catalytic activity. Characterization and performance in the reduction of methylene blue. Journal of Cleaner Production, 2019. **210**: p. 811-820.
14. Arnawtee, W.H., et al., Lignin valorization: Facile synthesis, characterization and catalytic activity of multiwalled carbon nanotubes/kraft lignin/Pd

nanocomposite for environmental remediation. Separation and Purification Technology, 2022. **290**: p. 120793.
15. Schauermann, S., et al., Nanoparticles for Heterogeneous Catalysis: New Mechanistic Insights. Accounts of Chemical Research, 2013. **46**(8): p. 1673-1681.
16. Narayan, N., A. Meiyazhagan, and R. Vajtai, Metal Nanoparticles as Green Catalysts. Materials, 2019. **12**(21).
17. Huang, N., Y. Xu, and D. Jiang, High-performance heterogeneous catalysis with surface-exposed stable metal nanoparticles. Scientific Reports, 2014. **4**(1): p. 7228.
18. Julis, J., M. Hölscher, and W. Leitner, Selective hydrogenation of biomass derived substrates using ionic liquid-stabilized ruthenium nanoparticles. Green Chemistry, 2010. **12**(9): p. 1634-1639.
19. Negui, M., et al., Wood-Sourced Polymers as Support for Catalysis by Group 10 Transition Metals. Processes, 2022. **10**(2).
20. Orooji, Y., et al., Valorisation of nuts biowaste: Prospects in sustainable bio(nano)catalysts and environmental applications. Journal of Cleaner Production, 2022. **347**: p. 131220.
21. Sajjadi, M., et al., Lignin-derived (nano)materials for environmental pollution remediation: Current challenges and future perspectives. International Journal of Biological Macromolecules, 2021. **178**: p. 394-423.
22. Nasrollahzadeh, M., et al., Recent progresses in the application of lignin derived (nano)catalysts in oxidation reactions. Molecular Catalysis, 2020. **489**: p. 110942.
23. Hussain, F., et al., Waste animal bones as catalysts for biodiesel production; a mini review. Catalysts, 2021. **11**(5): p. 630.
24. Nasrollahzadeh, M., et al., Low-cost and sustainable (nano)catalysts derived from bone waste: catalytic applications and biofuels production. Biofuels, Bioproducts and Biorefining, 2020. **14**(6): p. 1197-1227.
25. Konwar, M., M. Chetia, and D. Sarma, A Low-Cost, Well-Designed Catalytic System Derived from Household Waste “Egg Shell”: Applications in Organic Transformations. Topics in Current Chemistry, 2019. **377**(1): p. 6.
26. Budžaki, S., et al., Waste Management in the Agri-Food Industry: The Conversion of Eggshells, Spent Coffee Grounds, and Brown Onion Skins into Carriers for Lipase Immobilization. Foods, 2022. **11**(3).
27. Nasrollahzadeh, M., S.M. Sajadi, and A. Hatamifard, Waste chicken eggshell as a natural valuable resource and environmentally benign support for biosynthesis of catalytically active Cu/eggshell, Fe3O4/eggshell and Cu/Fe3O4/eggshell nanocomposites. Applied Catalysis B: Environmental, 2016. **191**: p. 209-227.
28. Balasooriya, I.L., et al., Applications of Nano Hydroxyapatite as Adsorbents: A Review. Nanomaterials (Basel), 2022. **12**(14).
29. Gomes, D., et al., A brief review on hydroxyapatite production and use in biomedicine. Cerâmica, 2019. **65**: p. 282-302.
30. Fihri, A., et al., Hydroxyapatite: A review of syntheses, structure and applications in heterogeneous catalysis. Coordination Chemistry Reviews, 2017. **347**: p. 48-76.
31. Shi, D., et al., Optimization of hydrothermal synthesis of hydroxyapatite from chicken eggshell waste for effective adsorption of aqueous Pb(II). Environ Sci Pollut Res Int, 2021. **28**(41): p. 58189-58205.
32. Engel, G. and W. Klee, Infrared spectra of the hydroxyl ions in various apatites. Journal of Solid State Chemistry, 1972. **5**(1): p. 28-34.
33. Saka, C., Ö. Şahin, and M.M. Küçük, Applications on agricultural and forest waste adsorbents for the removal of lead (II) from contaminated waters. International Journal of Environmental Science and Technology, 2012. **9**(2): p. 379-394.
34. Pramanik, S., et al., Development of high strength hydroxyapatite by solid-state-sintering process. Ceramics International, 2007. **33**(3): p. 419-426.
35. Choi, H.-J., Assessment of the adsorption kinetics, equilibrium and thermodynamic for Pb(II) removal using a hybrid adsorbent, eggshell and sericite, in aqueous solution. Water Science and Technology, 2019. **79**(10): p. 1922-1933.
36. Yan, Y., et al., A new low-cost hydroxyapatite for efficient immobilization of lead. Journal of Colloid and Interface Science, 2019. **553**: p. 798-804.
37. Kumar, T.S.S., K. Madhumathi, and R. Jayasree, Eggshell Waste: A Gold Mine for Sustainable Bioceramics. Journal of the Indian Institute of Science, 2022. **102**(1): p. 599-620.
38. Marwaha, A., et al., Waste materials as potential catalysts for biodiesel production: Current state and future scope. Fuel Processing Technology, 2018. **181**: p. 175-186.
39. Yadav, V.K., et al., The Processing of Calcium Rich Agricultural and Industrial Waste for Recovery of Calcium Carbonate and Calcium Oxide and Their Application for Environmental Cleanup: A Review. Applied Sciences, 2021. **11**(9).
40. Das, A. and D. Pamu, A comprehensive review on electrical properties of hydroxyapatite based ceramic composites. Materials Science and Engineering: C, 2019. **101**: p. 539-563.
41. Muthu, D., et al., Rapid synthesis of eggshell derived hydroxyapatite with nanoscale characteristics for biomedical applications. Ceramics International, 2022. **48**(1): p. 1326-1339.

42. Shi, D., et al., Optimization of hydrothermal synthesis of hydroxyapatite from chicken eggshell waste for effective adsorption of aqueous Pb(II). Environmental Science and Pollution Research International, 2021. **28**(41): p. 58189-58205.
43. Mohammad, M., F. Ahmadpoor, and S.A. Shojaosadati, Mussel-Inspired Magnetic Nanoflowers as an Effective Nanozyme and Antimicrobial Agent for Biosensing and Catalytic Reduction of Organic Dyes. ACS Omega, 2020. **5**(30): p. 18766-18777.
44. Mulongo-Masamba, R., et al., New functional β-chitin/calcium phosphate as promising support of copper nanocatalyst for the reductive degradation of methylene blue. International Journal of Environmental Science and Technology, 2019. **16**(12): p. 8117-8128.
45. Abdeta, A.B., et al., A novel AgMoOS bimetallic oxysulfide catalyst for highly efficiency catalytic reduction of organic dyes and Chromium (VI). Advanced Powder Technology, 2021. **32**(8): p. 2856-2872.
46. Pasinszki, T., et al., Copper nanoparticles grafted on carbon microspheres as novel heterogeneous catalysts and their application for the reduction of nitrophenol and one-pot multicomponent synthesis of hexahydroquinolines. New Journal of Chemistry, 2018. **42**(2): p. 1092-1098.
47. Xu, P., et al., A facile electrostatic droplets assisted synthesis of copper nanoparticles embedded magnetic carbon microspheres for highly effective catalytic reduction of 4-nitrophenol and Rhodamine B. Materials Chemistry and Physics, 2020. **253**: p. 123444.
48. Rath, P.C., et al., Exceptional catalytic performance of ultrafine Cu2O nanoparticles confined in cubic mesoporous carbon for 4-nitrophenol reduction. Applied Surface Science, 2018. **427**: p. 1217-1226.

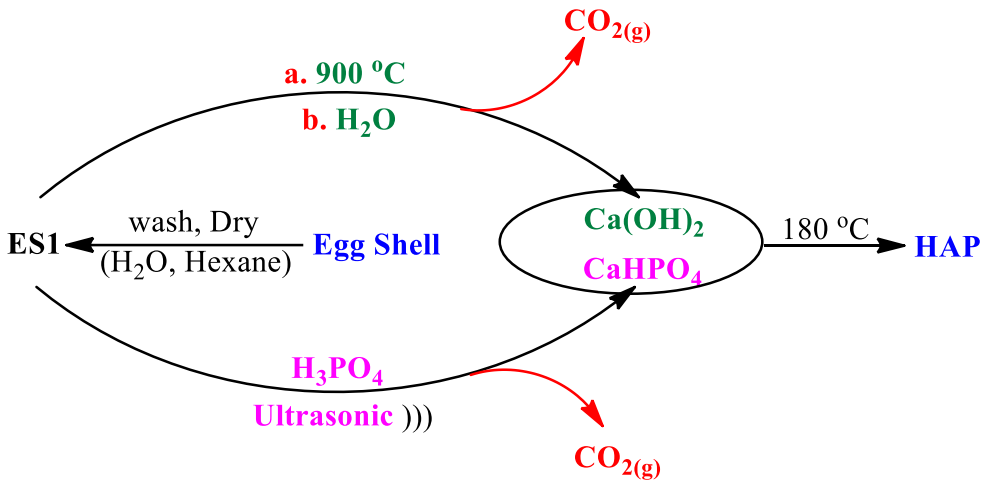

Scheme 1. A demonstration of the involved reactions to the preparation of eggshell derived HAP.

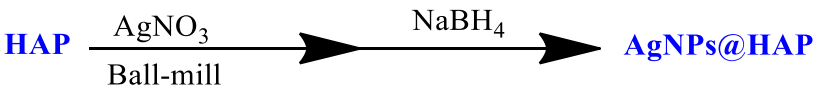

Scheme 2. The preparation of AgNPs@HAP from eggshell-derived HAP

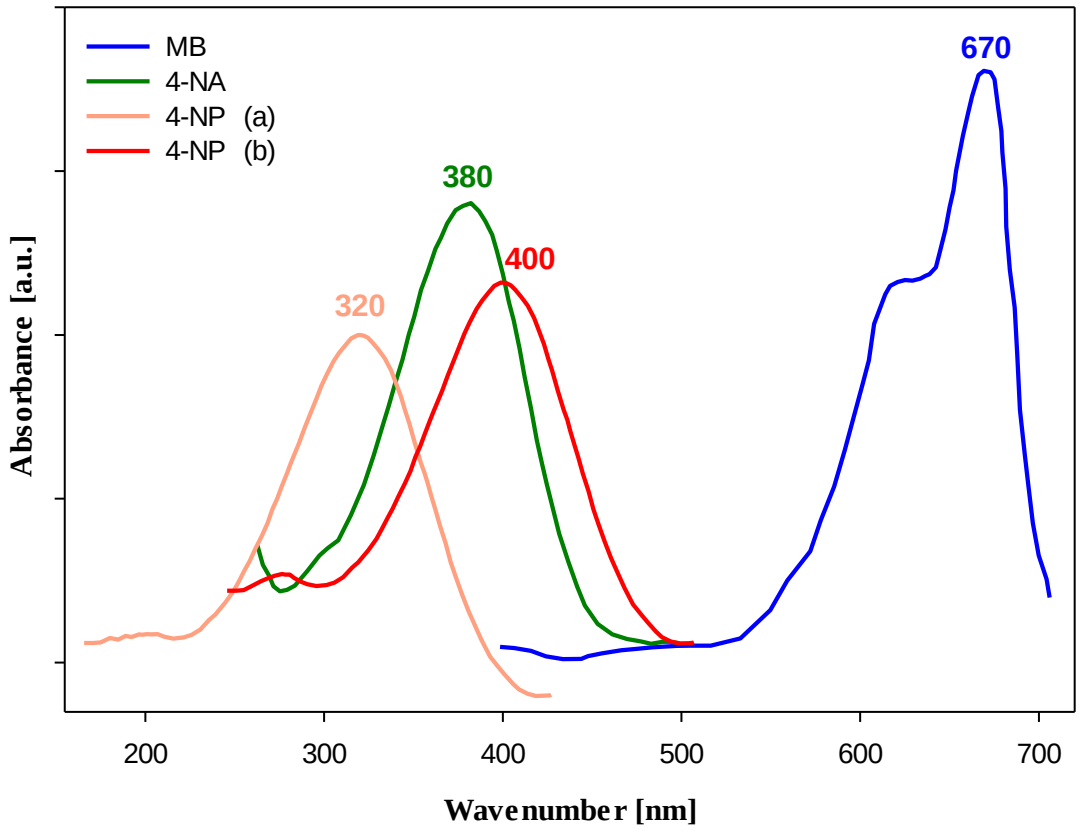

Figure 1. The corresponded λ_{max} of applied OPDs (MB, 4-NP and 4-NA).

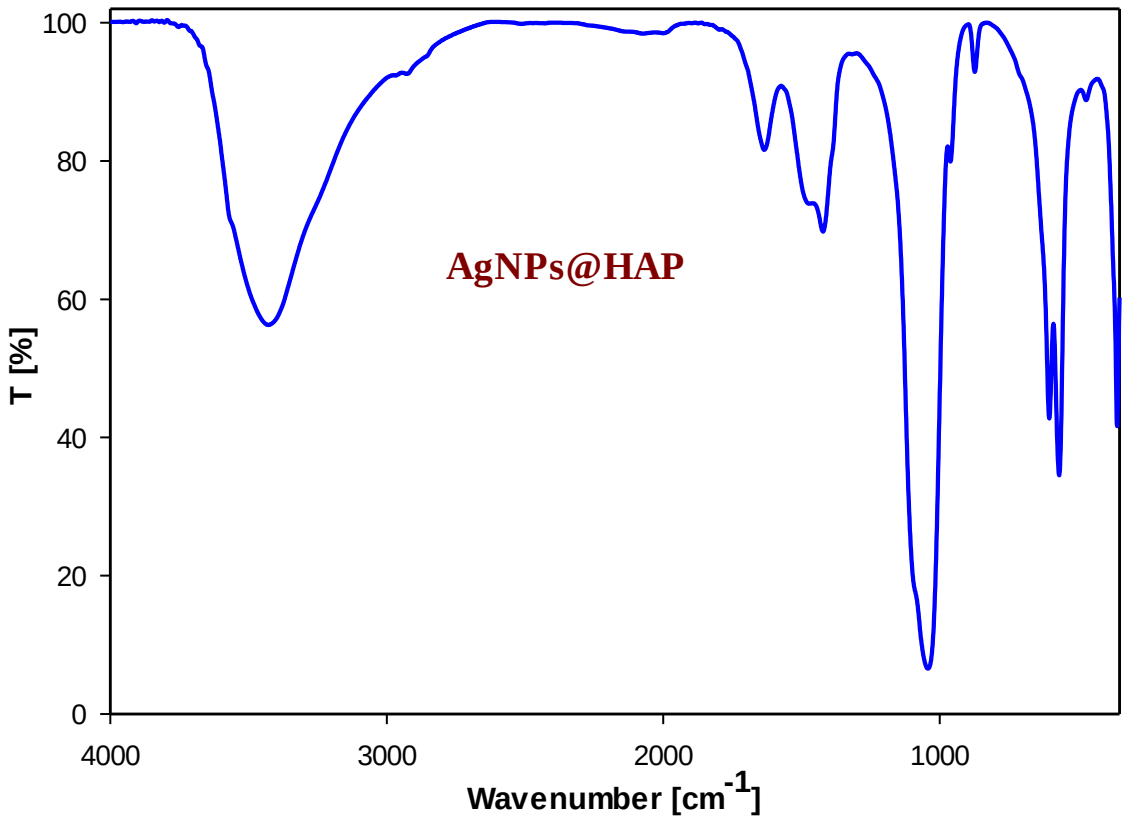

Figure 2. FT-IR spectra of AgNPs@HAP

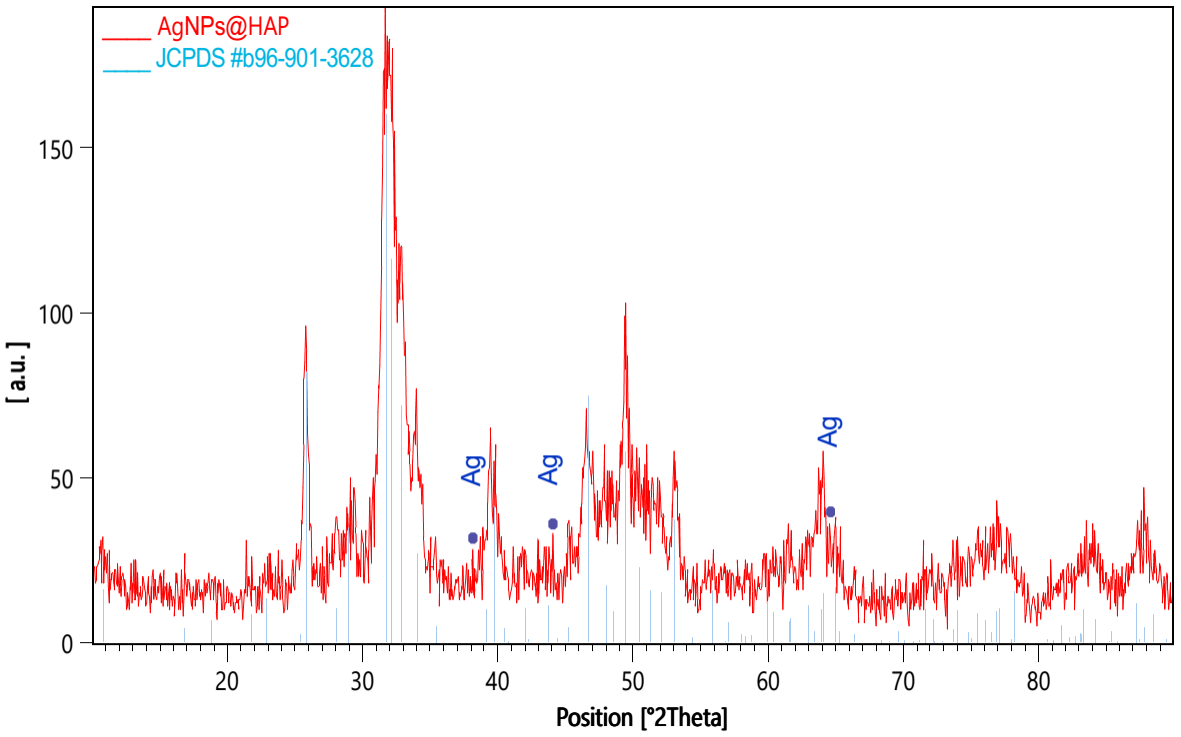

Figure 3. XRD pattern of AgNPs@HAP and JCPDS #b96-901-3628.

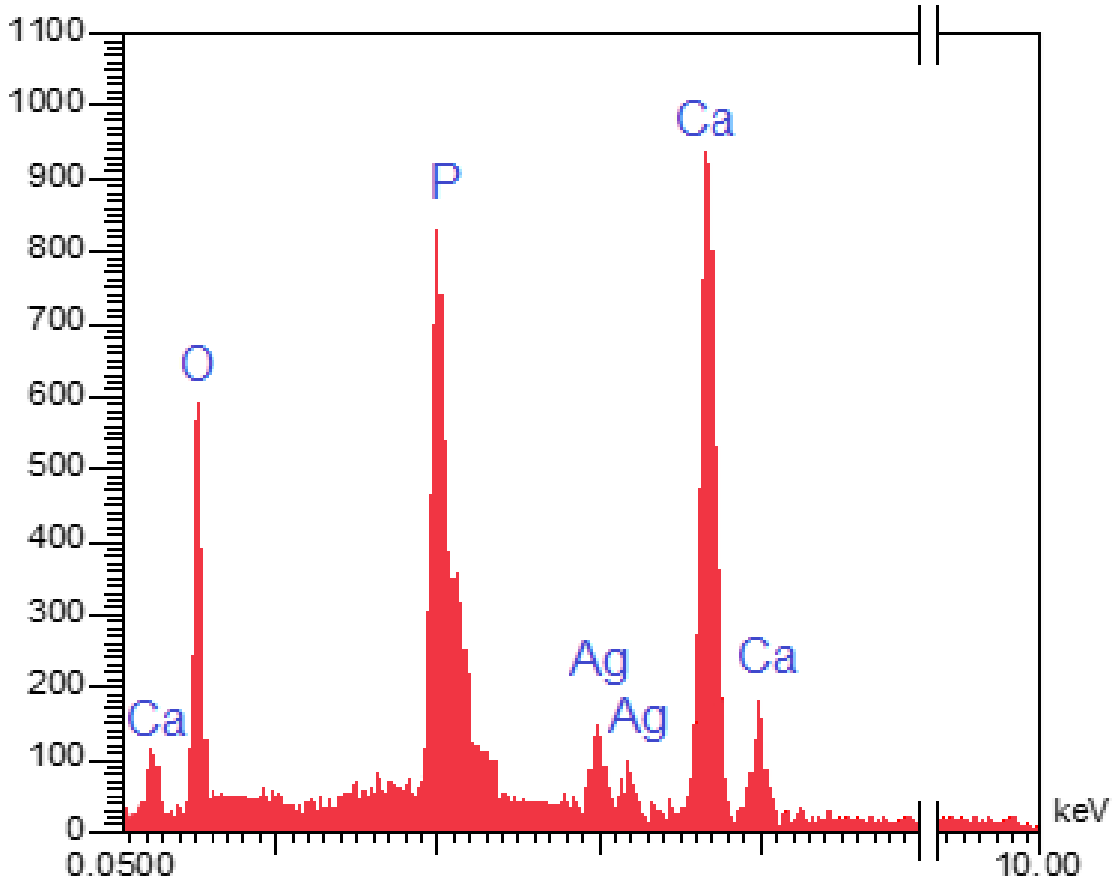

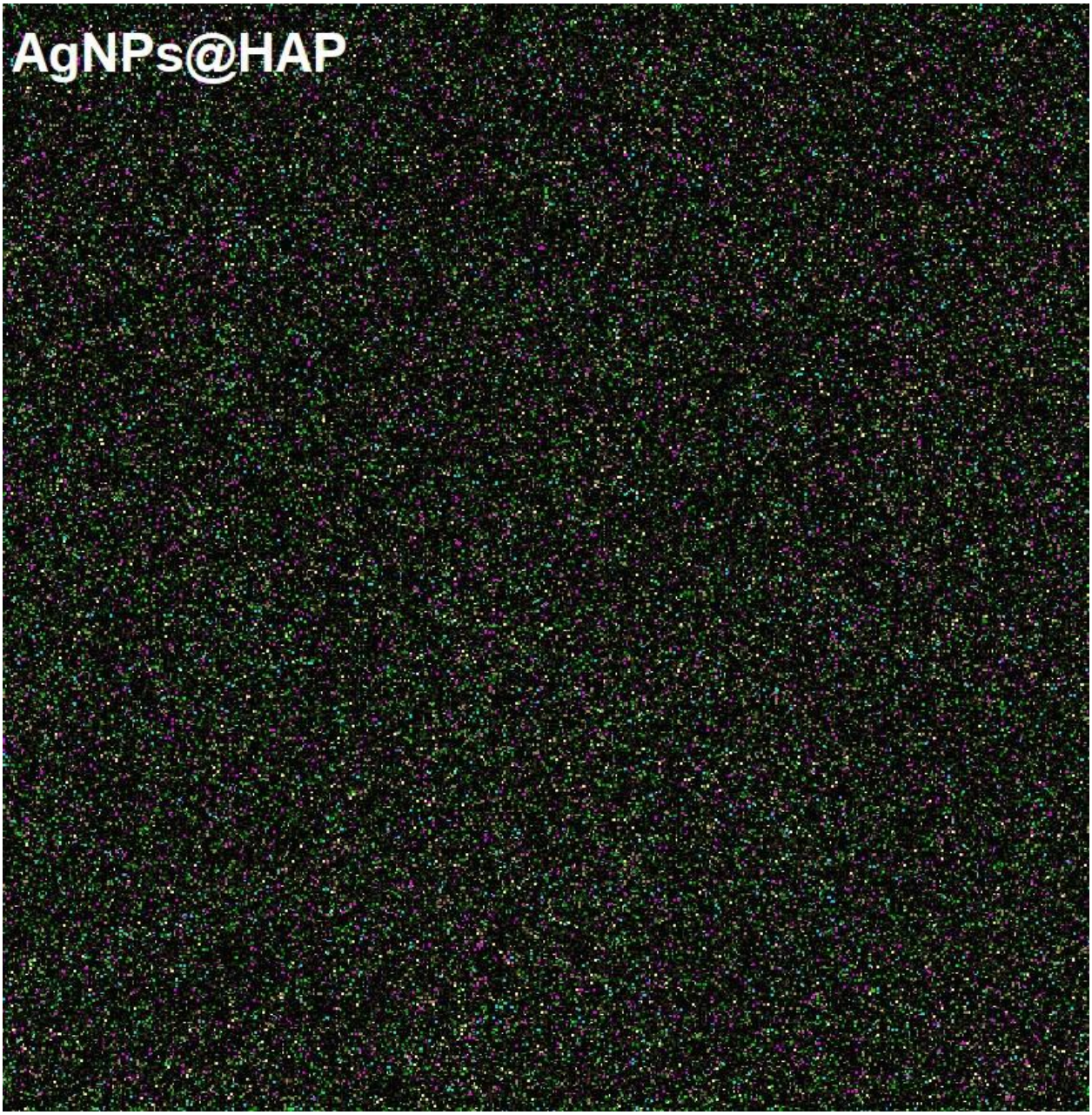
AgNPs@HAP

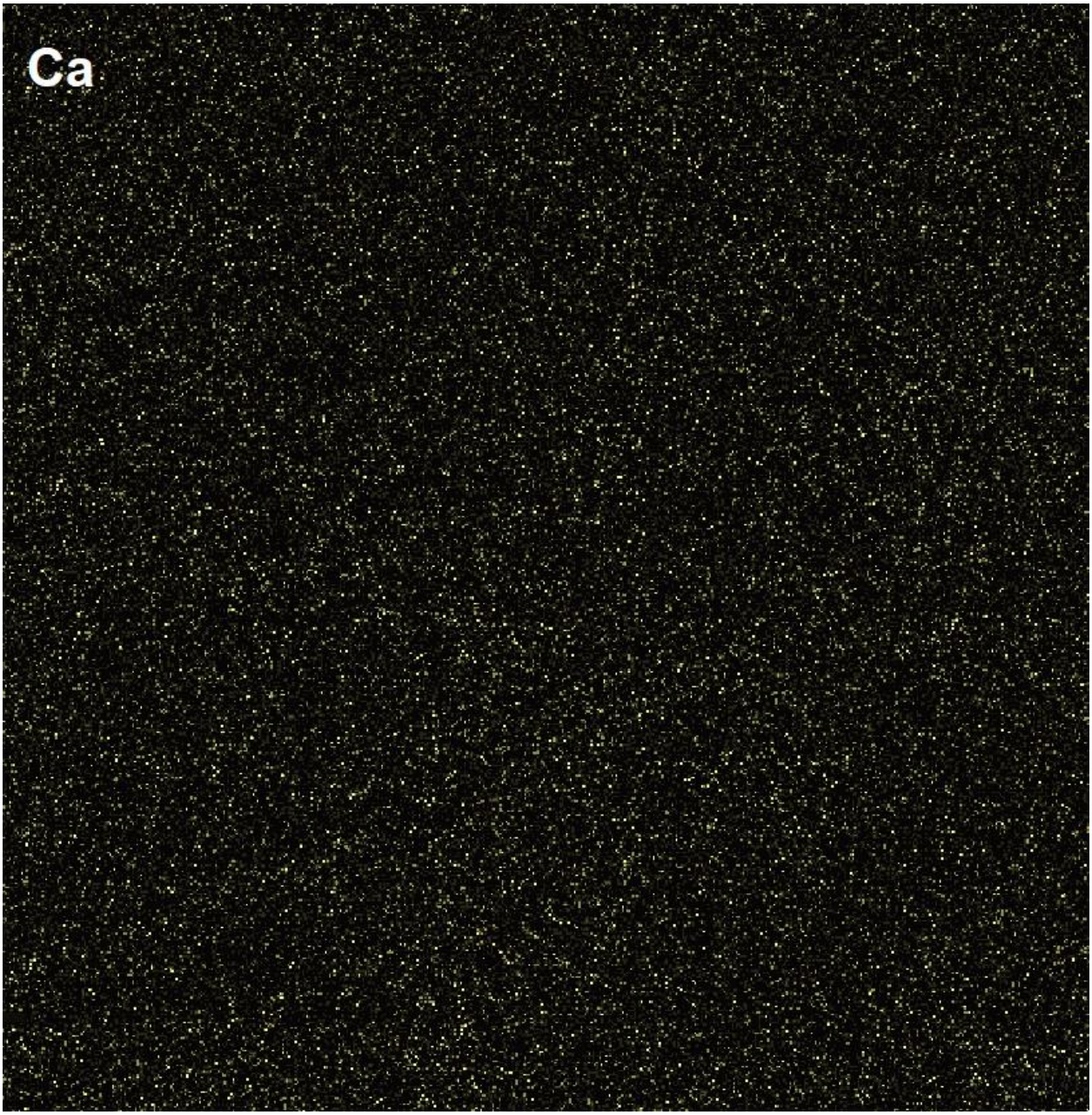
Ca

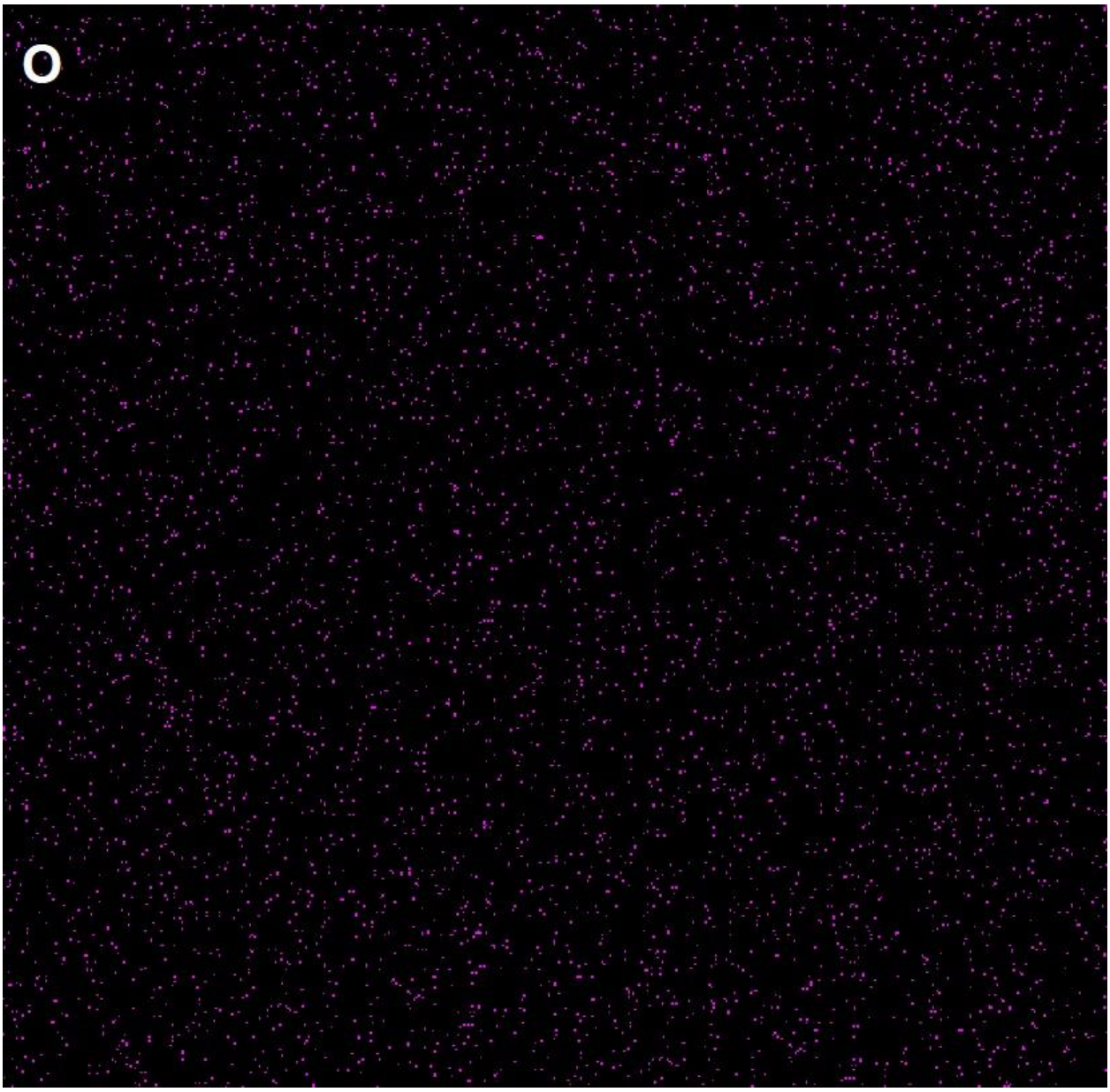
O

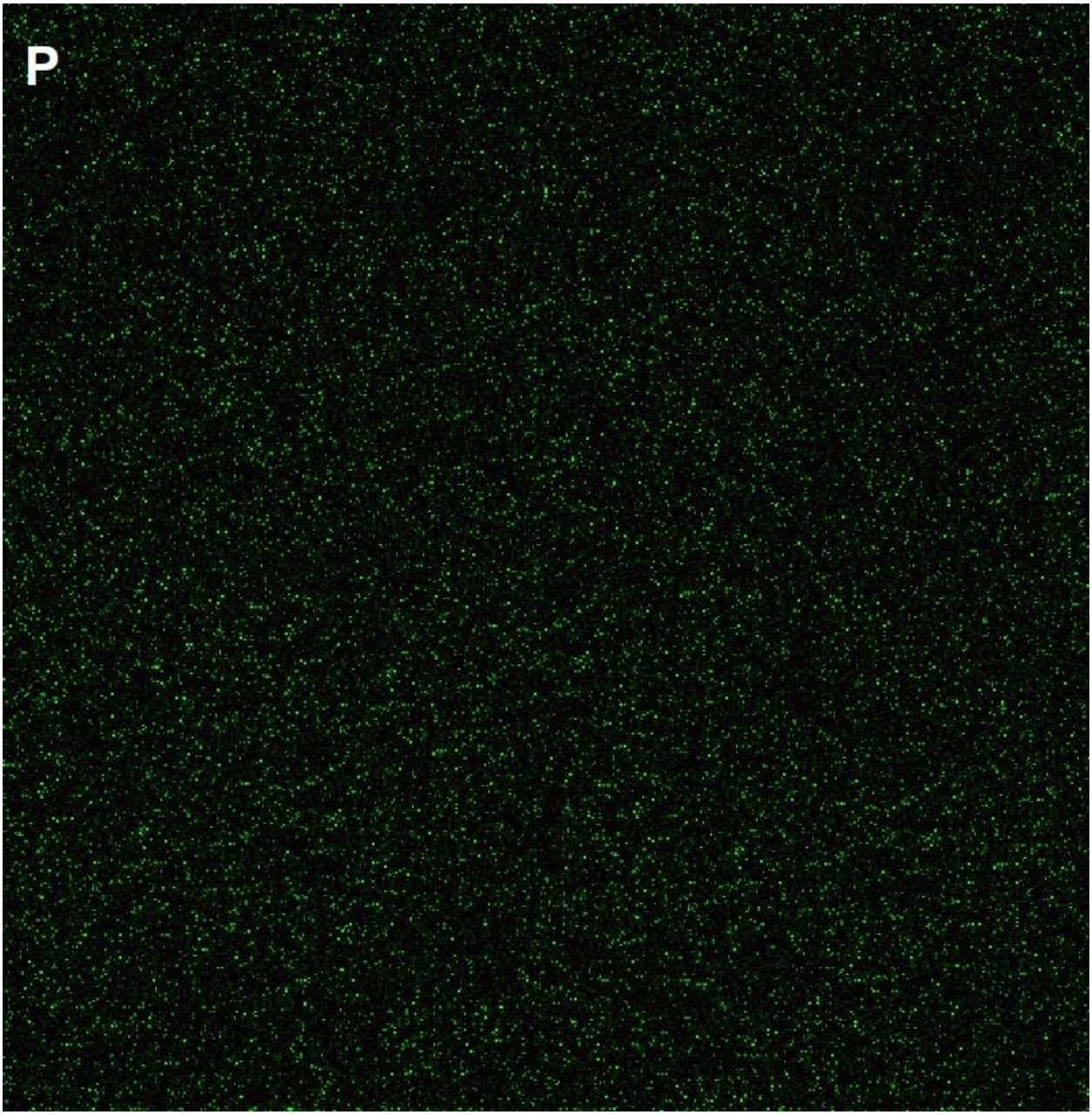
P

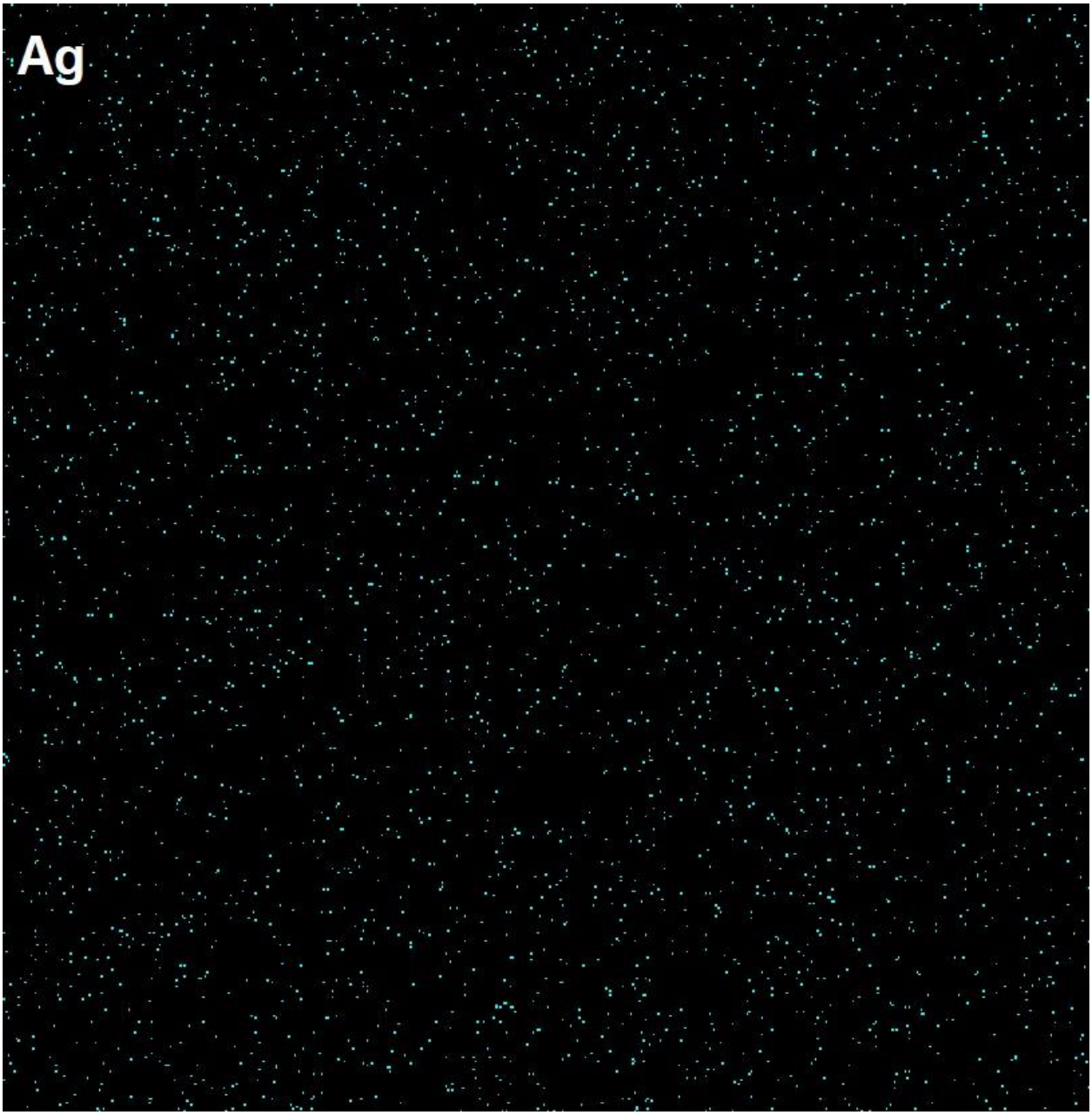

Figure 4. EDS analysis and elemental mapping of AgNPs@HAP.

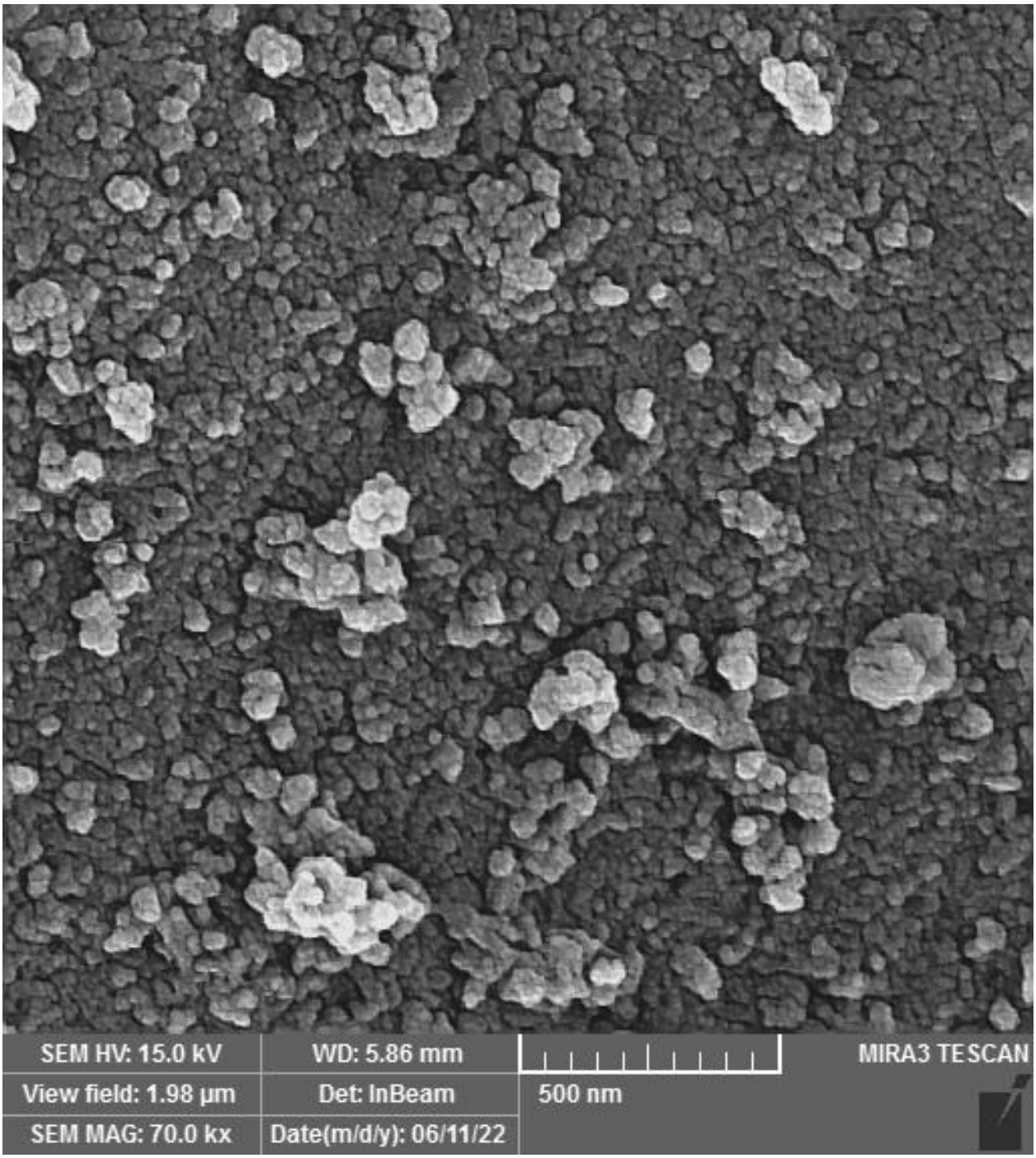
SEM HV: 15.0 kV
WD: 5.86 mm
MIRA3 TESCAN
View field: 1.98 µm
Det: InBeam
500 nm
SEM MAG: 70.0 kx
Date(m/d/y): 06/11/22

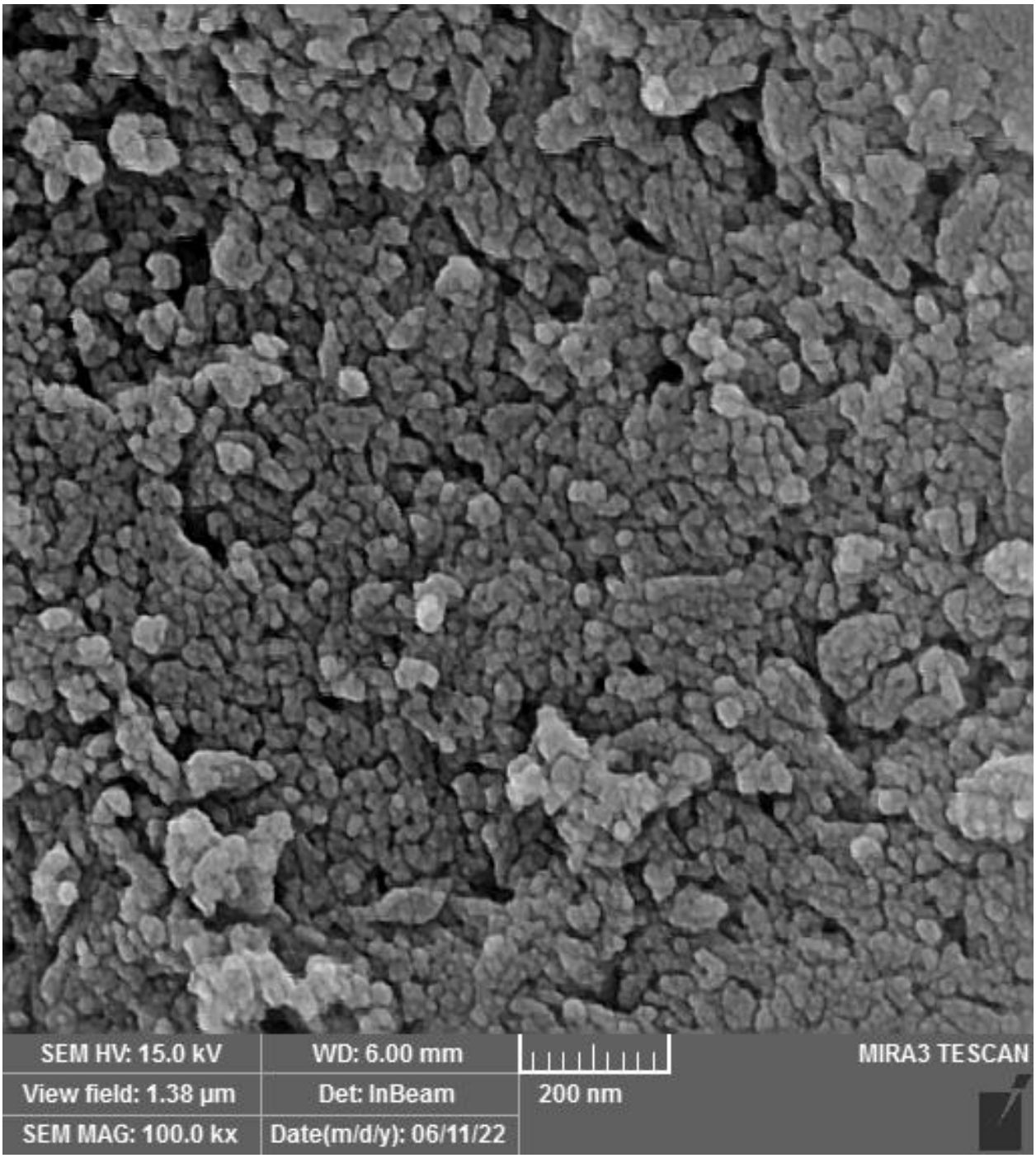

Figure 5. FESEM images of AgNPs@HAP.

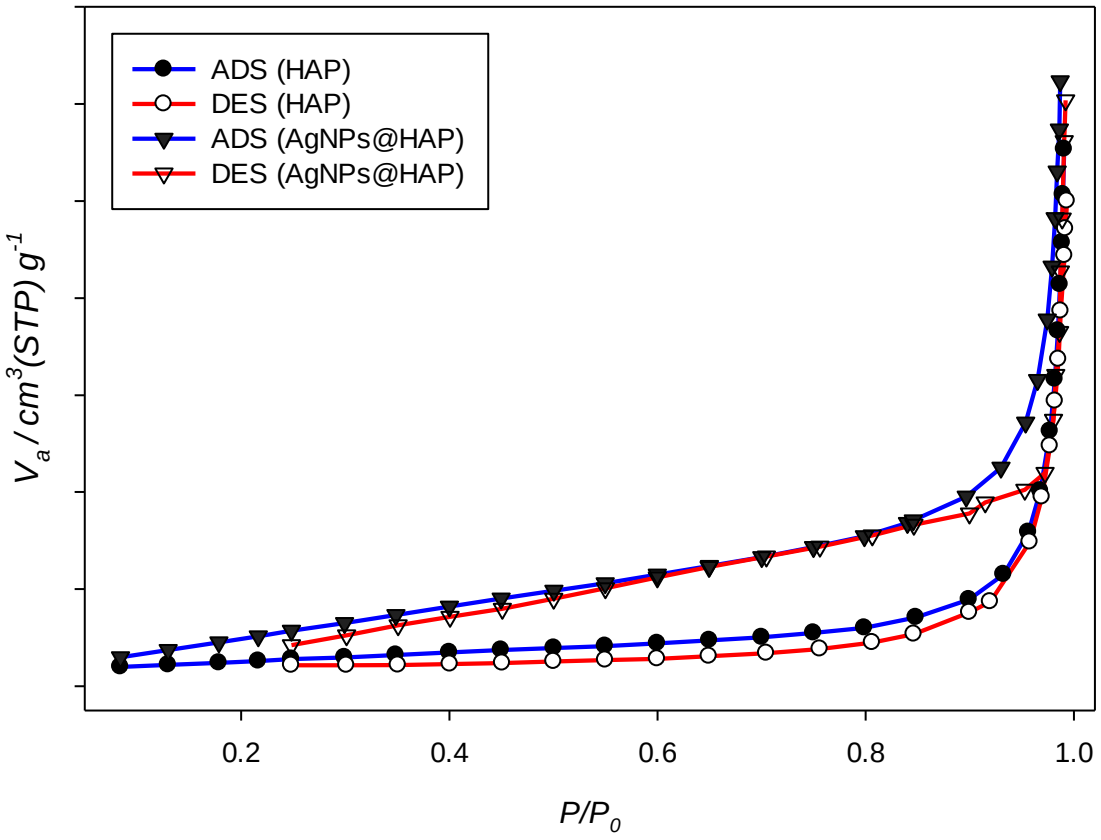

Figure 6. N_2 adsorption-desorption isotherms of HAP and AgNPs@HAP.

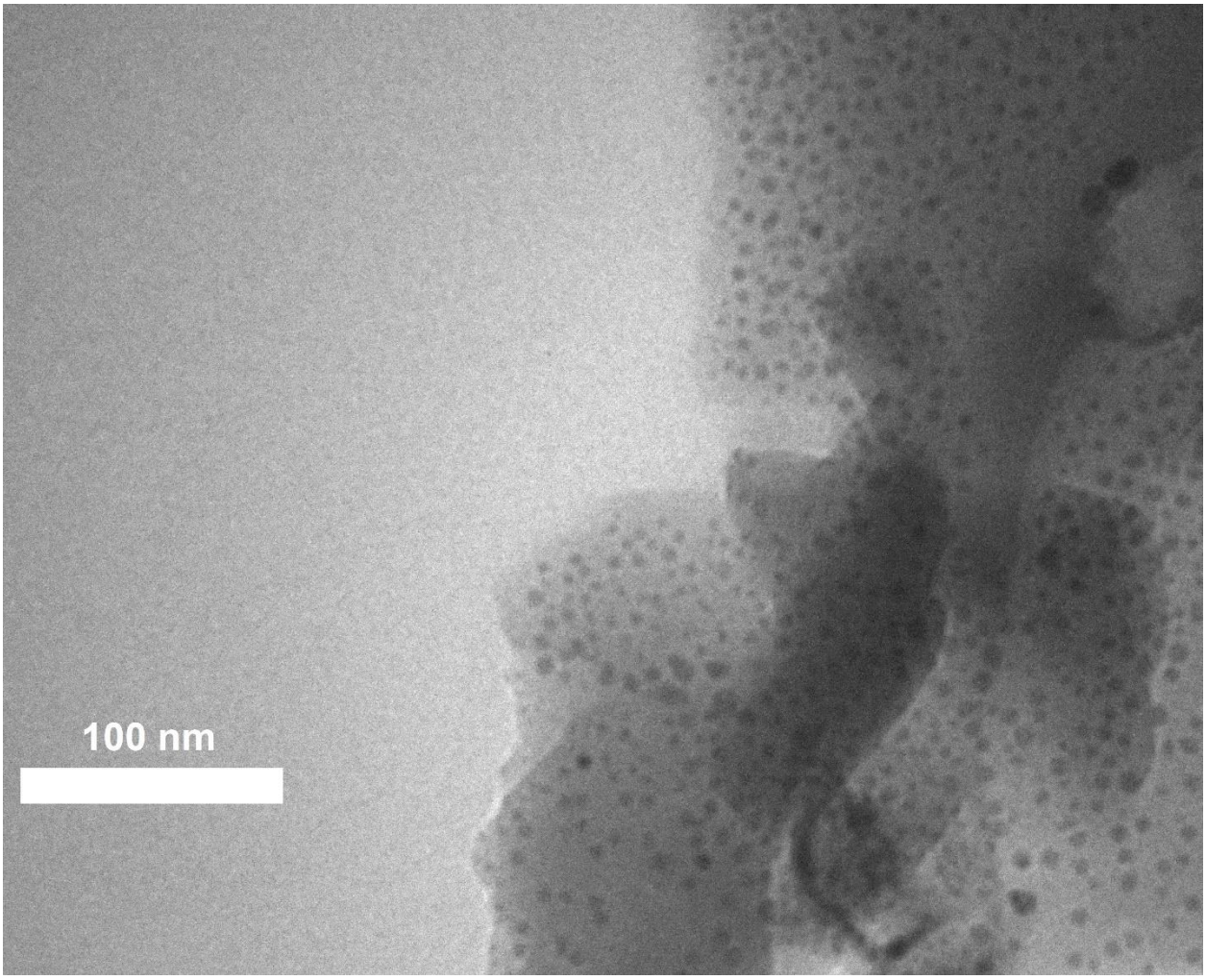
100 nm

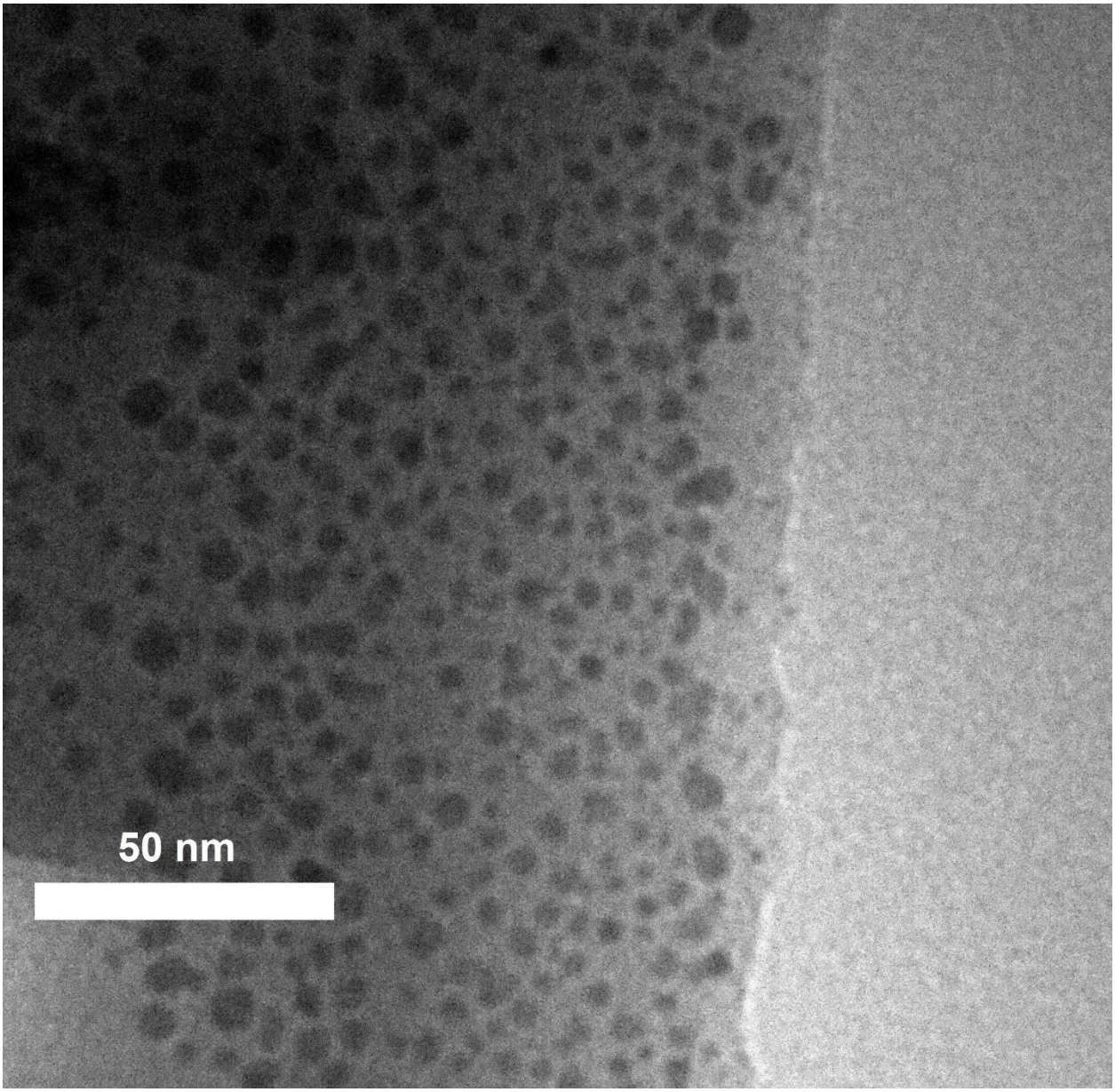

Figure 7. TEM images of AgNPs@HAP.

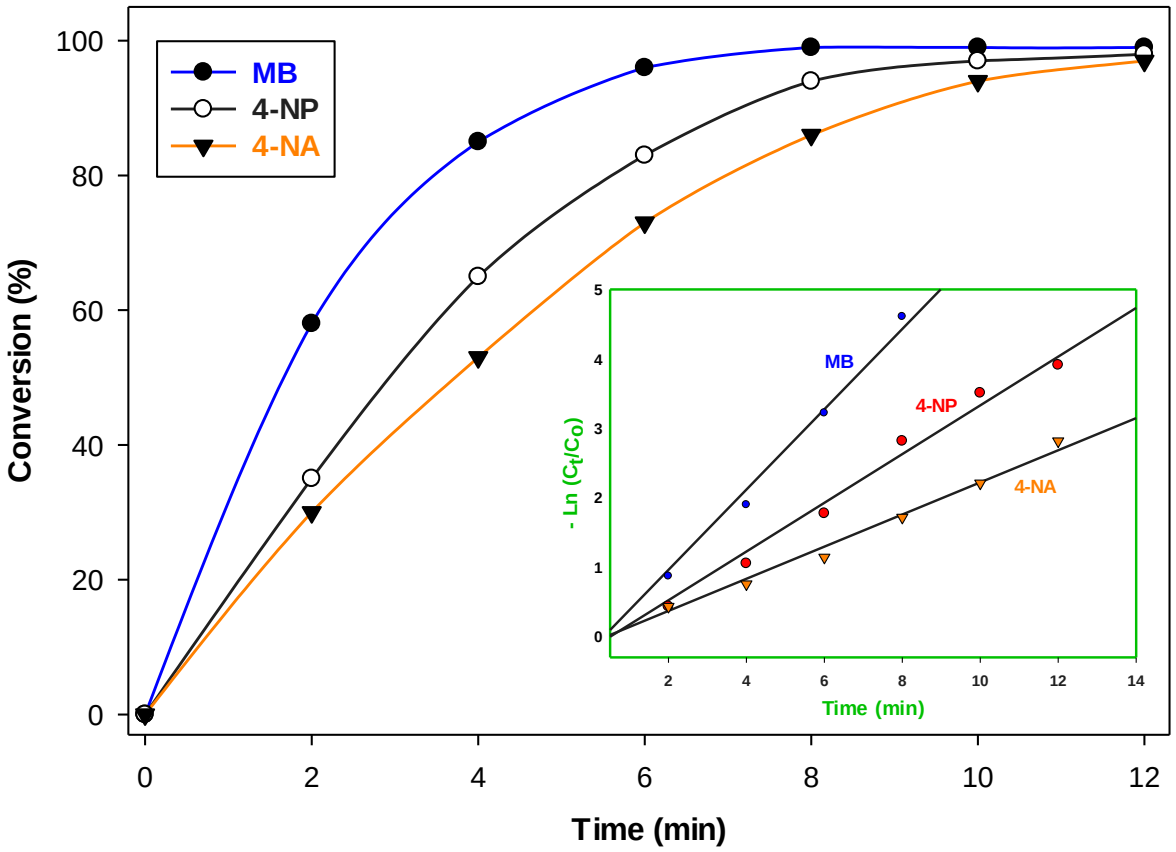

Figure 8. The relationship between reaction conversion (%) and Plotting of –Ln ($[C_t]/[C_o]$) versus operation reaction time (min) during the catalytic reduction reaction of corresponded organic dyes (MB: R^2=0.990 and k=0.578; 4-NP: R^2= 0.987 and k=0.352; 4-NA: R^2=0.979, k=0.297) in the presence of $NaBH_4$.

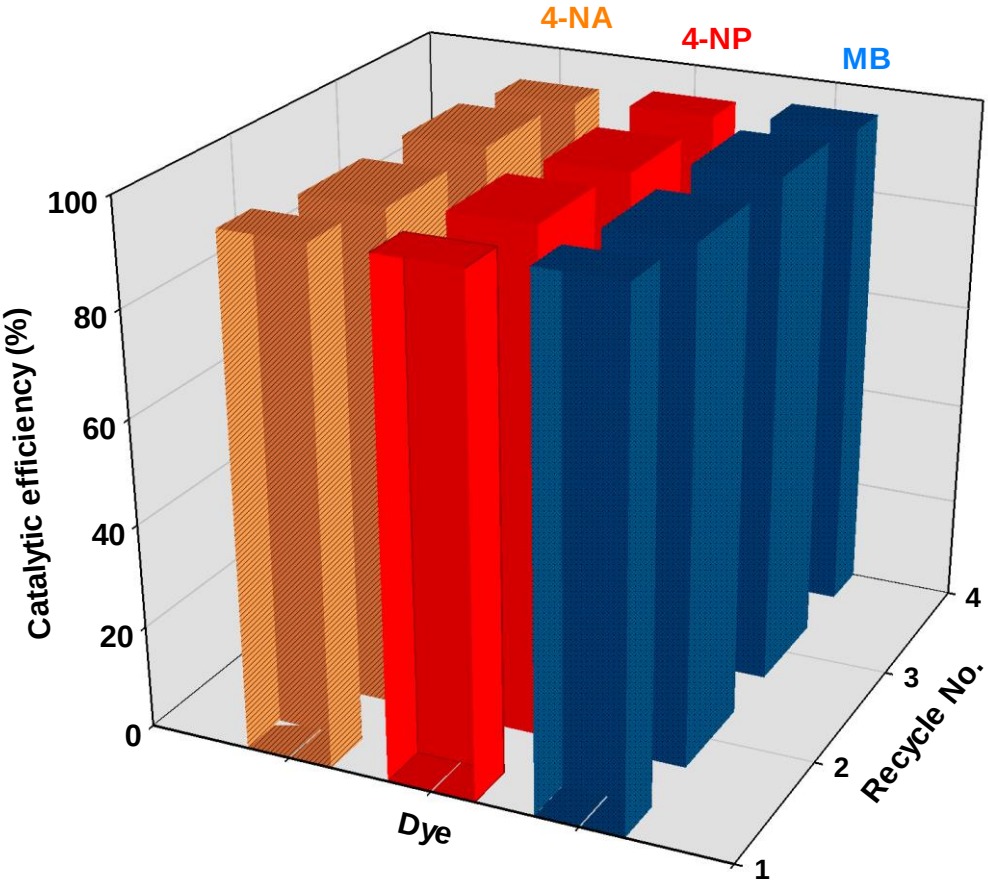

Figure 9. The catalytic efficiency of recycled AgNPs@HAP in the reduction reaction of organic dyes (MB, 4-NP and 4-NA)

Table 1. Textural properties of HAP and AgNPs@HAP[a]

Sample	S_{BET} (m^2 g^{-1})	TPV (cm^3(STP) g^{-1})	Mpd. (nm)
HAP	62.15	0.61	28.41
AgNPs@HAP	56.03	0.47	31.08

[a]TPV: Total Pore Volume; Mpd: Mean pore diameter.

Table 2. Comparison of catalytic reduction of MB and 4-NP in the presence of various catalysts.

Catalyst	Catalyst dosage (mg)	Pollutant	Pollutant Conc. (ppm)	$NaBH_4$ (M)	Time (min)	k (min^{-1})	Ref.
MPD-Cu nanoflowers[a]	0.4	MB	200 (0.1 mL)	3 (0.66 mL)	5 min	1.44	[43]
Cu(NPs)/β-CCP[b]	10	MB	16 (2 mL)	0.04 (0.5 mL)	4 min	0.57	[44]
Cu@SBA-15	1	MB	8.95 (22.5 mL)	0.2 (5 mL)	8 min	0.51	[45]
AgNPs@HAP	**0.6**	**MB**	**40 (25 mL)**	**0.1 (30 mL)**	**8**	**0.578**	**This work**
Cu-NP/C microspheres	4	4-NP	27.8 (1.5 mL)	0.02 (1.5 mL)	6 min	0.3	[46]
Cu/MC microspheres	0.5	4-NP	42 (6 mL)	0.5 (2 mL)	5 min	0.96	[47]
CuO@cubic carbon	0.2	4-NP	12.5 (22.5 mL)	0.05 (5 mL)	6 min	1.32	[48]
AgNPs@HAP	**0.8**	**4-NP**	**20 (25 mL)**	**0.1 (30 mL)**	**10**	**0.352**	**This work**

[a]Magnetic polydopamine-Cu nanoflowers, [b]Cu(NPs)/β-chitin/dicalcium phosphate